Accepted Manuscript

Porous MoO_2-Cu/C/Graphene nano-octahedrons quadruple nanocomposites as an advanced anode for lithium ion batteries with enhanced rate capability

Kaixuan Zhang, Hongxun Yang, Minfeng Lü, Chao Yan, Huipeng Wu, Aihuan Yuan, Shengling Lin

PII: S0925-8388(17)33525-9

DOI: 10.1016/j.jallcom.2017.10.091

Reference: JALCOM 43488

To appear in: *Journal of Alloys and Compounds*

Received Date: 24 June 2017

Revised Date: 11 October 2017

Accepted Date: 12 October 2017

Please cite this article as: K. Zhang, H. Yang, M. Lü, C. Yan, H. Wu, A. Yuan, S. Lin, Porous MoO_2-Cu/C/Graphene nano-octahedrons quadruple nanocomposites as an advanced anode for lithium ion batteries with enhanced rate capability, *Journal of Alloys and Compounds* (2017), doi: 10.1016/j.jallcom.2017.10.091.

Graphical abstract

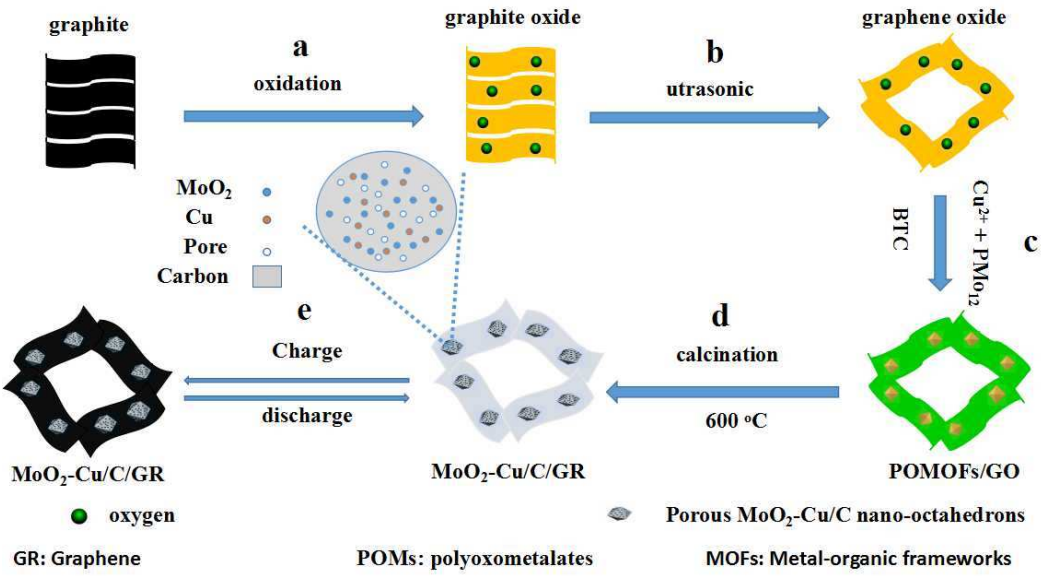

Porous MoO_2-Cu/C/Graphene nano-octahedrons quadruple nanocomposites as an advanced anode for lithium ion batteries with enhanced rate capability

Kaixuan Zhang[a, b, e], *Hongxun Yang*[a, b, d,*], *Minfeng Lü*[a], *Chao Yan*[c], *Huipeng Wu*[a, d], *Aihuan Yuan*[a, b], *and Shengling Lin*[a,*]

[a]*School of Environmental & Chemical Engineering, Jiangsu University of Science and Technology, Zhenjiang 212003, Jiangsu, China,* [b]*Marine Equipment and Technology Institute, Jiangsu University of Science and Technology, Zhenjiang 212003, Jiangsu, China,* [c]*School of Material Science and Engineering, Jiangsu University of Science and Technology, Zhenjiang 212003, China,* [d]*Jiangsu Tenpower Lithium Co. Ltd., Zhangjiagang 215618, Jiangsu, China,* [e]*State Key Laboratory of Structural Chemistry, Fujian Institute of Research on the Structure of Matter, Chinese Academy of Sciences, Fujian, Fuzhou, 350002, China,*

*Corresponding author: E-mail address: yhongxun@126.com (Hongxun Yang); and

*Corresponding author: E-mail address: linshl5757@sina.com (Shengling Lin)

ABSTRACT: A new porous MoO_2-Cu/C/graphene quadruple nanocomposite was designed and synthesized by a facile one-pot chemical precipitation method followed by calcination. As an anode for lithium ion batteries, the porous MoO_2-Cu/C/graphene nanocomposite delivers a high reversible capacity with significantly enhanced cycling stability (1114.8 mAh g^{-1} after 100 cycles at 0.1 A g^{-1}) and rate capability (892.6 mAh g^{-1} and 702.2 mAh g^{-1} at 1 A g^{-1} and 2 A g^{-1}, respectively). The greatly improved performances could be attributed to the positive synergistic effect of MoO_2 nano-octahedrons, Cu, carbon network derived from metal-organic framework, and graphene: the MoO_2 nano-octahedrons as lithium storage active materials, Cu phase as excellent conductor to improve the rate capability, the in-situ electrochemically carbon network as conductor and spacer to improve the rate capability and buffer the volume changes, and graphene as an efficient three dimensional conductive network to further accommodate the volume change of electrode materials.

Keywords: Molybdenum dioxide, Copper, Carbon, Graphene, Lithium ion batteries

1. Introduction

Transition metal oxides with higher theoretical capacity compared to currently commercial graphite, such as MoO_2 [1-9], Fe_2O_3 [10-13], Co_3O_4 [14-17], SnO_2 [18-20], ZnO [21-22], CuO [23-24], and TiO_2 [25-26], et al. have been proven to be promising candidates as advanced anodes for the next generation high power lithium ion batteries (LIBs). Among various anode materials, molybdenum dioxide (MoO_2) with high energy density (838 mAh g^{-1}) and low electrical resistivity has recently drawn much attention in LIBs [8, 9]. However, the rapid decay in capacity caused by the large volume variations upon charge-discharge processes and limited rate performance because of its inherent poor electrical conductivity impede its practical applications. To circumvent these challenges, popular strategy is to integrate active oxide materials into conductive matrices or scaffolds, such as carbon, metals, or graphene [27]. Recently, Xia group synthesized MoO_2@C composite in which carbon could enhance the electrical conductivity and protect MoO_2 anode, showing an improvement capacity of 1442 mAh g^{-1} after 50 cycles at 0.1 A g^{-1} rate and 443.8 mA h g^{-1} after 50 cycles at 1 A g^{-1} [4]. The improved electrochemcial properties of MoO_2@C composite is ascribed to the carbon which could protect the active materials and enhance the electrical conductivity. On the other hand, graphene (GR) is a famous star material for energy devices because of its superior electrical conductivity, high surface area, structural flexibility, and chemical tolerance [28-34]. Graphene-based hybrid such as Co_3O_4/graphene [32], Sn-In/graphene [33], Sn@C/graphene [34] and MoO_2/graphene [9] have been reported as anodes for LIBs to improve the reversible capacity and cycle performances. In those cases, graphene could not only prevent the aggregation of active electrode materials and accommodate the volume variations during cycling, but also decrease the contact resistance of active nanomaterials. In addition, various metal (including Cu, Co, Ag, etc.) phase can also promote the transport of electrons and facilitate the electrochemical reaction kinetics of hybrid electrode materials [33-38]. Huang et al. successfully synthesized $Li_4Ti_5O_{12}$/Cu composite by a facile solvothermal route, and the composite showed an improvement capacity of 141.6 mAh g^{-1} after 10 cycles at 10 C [35]. Based on above considerations,

it is highly desirable to synthesize a new nanocomposite as anodes for LIBs to fully combine the advantages of MoO_2, metal phase, carbon network, and GR. However, the development of a simple and effective method for the design of a quadruple MoO_2-Cu/C/GR nanocomposite with the satisfactory performances still remains a big challenge.

Recently, polyoxometalate-based metal-organic framework (POMOF) hybrid has also been studied for potential applications in catalysis and energy devices due to their high specific surface area, extra chemical composition, porous structure, versatile organic fragments, and high thermal stability [4, 5, 39-48]. For instance, two isostructural POMOF with diamond topology, NENU-506 and NENU-507, exhibited high reversible capacity of 640 mA h g^{-1} after 100 cycles, when applied as an anode for LIBs [44]. Lan et al. also reported a POMOF consisting of Zn-3-Keggin fragments connected with tris-(4-pyridyl)triazine) ligands exhibited a highly reversible capacity of 750 mAh g^{-1} at 50 mA g^{-1} after 200 cycles with excellent cycle stability and rate performance [46]. On the other hand, metal oxides can be obtained via controlled pyrolysis of POMOF precursor [4, 5, 47]. Porous MoO_3@CuO derived from POMOF demonstrates good performance and excellent cycle life due to the layered structure of MoO_3 providing facilitated ion transport and electron diffusion pathways for the composite material [47]. Lin et al. synthesized a composite of MoO_2@Cu@C using a thermolysis template of POMOF crystal, exhibiting an excellent capacity of 28.33 mAh g^{-1} at 1 A g^{-1} in supercapacitors [5]. Dispite those progresses, MoO_2-Cu/C/GR nanocomposites derived-POMOF/graphene oxide (GO) precursor as anode materials for LIBs have not been reported.

Herein, we report a new MoO_2-Cu/C/GR quadruple nanocomposite arived from POMOF/GO precursor which contains phosphomolybdic acid hydrate, graphene, and Cu-based MOFs forming intriguing structures. As an advanced anode for LIBs, porous MoO_2-Cu/C/GR nano-octahedrons exhibited a large reversible capacity, obvious improvement in capacity retentions and rate capability.

2. Experimental section

2.1. Synthesis of the MoO_2-Cu/C/GR nano-octahedrons

All chemicals are of analytical grade, and were used without any further purification. Graphene oxide (GO) was synthesized from graphite by a modified Hummers method [33, 49]. 0.996 g copper (II) acetate monohydrate, 0.073 g L-glutamic acid and 0.421 g phosphomolybdic acid hydrate (POM) were dissolved in 50 mL distilled water and stirred at ambient condition for 30 mins as solution A. 50 mg graphene oxide was dispersed in 50 mL ethanol by ultrasonic cleaner for 1 h at room temperature, then 0.138 g 1, 3, 5-benzenetricarboxylic acid (BTC) was added under continuous stirring as solution B. Then solution B was poured into solution A with continuous stirring and a precipitate appeared immediately. After being stirred for 24 h, the precipitation was washed with ethanol and distilled water for three times and then was dried in vacuum at 60 ^{o}C to get POMOF/GO. The POMOF/GO was contained at 600 ^{o}C for 3 h with a ramp rate of 2 ^{o}C min^{-1} under N_2 atmosphere to get the target product. Finally, the product was taken out and the color changed from green to black. For comparison, porous MoO_2-Cu/C was prepared via POMOF precursor under similar conditions without the presence of GO. Porous MoO_2/C was synthesized using MoO_2-Cu/C by $FeCl_3$ etching [39].

2.2. Material characterizations

The morphologies and structures of the as-synthesized product were characterized by a X-ray diffraction (XRD) analyzer (Shimadzu XRD-6000 diffractometer using Cu-Kα radiation (0.15406 nm), a scanning electron microscope (JEOL, JSM-6700 F, 5 kV), transmission electron microscope (TEM, JEOL JEM-1400), high-resolution transmission electron microscopy (HRTEM) images and element mapping results were performed on FEI F20 S-TWIN at an acceleration voltage of 200 kV. Raman spectra were carried on a Renishaw Raman spectrometer. The BET surface area of the as-obtained sample was determined by an ASAP 2020 surface analyzer at 77 K. Pore size distribution analysis was based on the Barrett-Joyner Halenda (BJH) results. Thermogravimetric analysis (TGA) was carried out using a Labsys Evo thermoanalyser under Air flow. X-ray photoelectron spectroscopy (XPS) measurement was performed on a ESCALAB 250XI spectrometer with monochromatic Al Ka as the X-ray source. Mo and Cu were

determined by a Jobin Yvon Ultima2 ICP atomic emission spectrometer. Anal. calcd. for MoO_2-Cu/C/GR: Mo, 59.1%; Cu, 9.8 %.

2.3. Electrochemical measurements

The working electrodes were prepared by mixing 80wt% MoO_2-Cu/C/GR , 10wt% Super P, and 10wt% polyvinylidene fluoride dissolved in N-methyl-2-pyrrolidinone. The resulting slurry was pasted onto copper foil and dried in a vacuum oven Coin-type half cells (2032R-type), the MoO_2-Cu/C/GR as working electrode, lithium metal ascount erelectrode and 1M $LiPF_6$ in ethylene carbonate/diethyl carbonate (1:1 vol%) as electrolyte. The active mass loading on the electrode is about 1.04 mg cm^{-2}. The electrochemical properties of the MoO_2-Cu/C/GR nanocomposites were evaluated via a battery cycle tester (LAND CT-2001A, Wuhan, China). Cyclic voltammetry (CV) was measured by an electrochemical workstation (CHI 760 E, Chenhua Ltd. Co., China) between 3.0 and 0.01 *vs* (Li/Li^+)/V at 0.2 mV s^{-1} sweep rate. Electrochemical impedance spectroscopy (EIS) tests were carried out on an electrochemical workstation (Autolab 302 N) in the frequency range of 0.1 Hz to 10^6 Hz with *ac* amplitude of 10 mV.

3. Results and discussion

3.1. Characterizations of MoO_2-Cu/C/GR

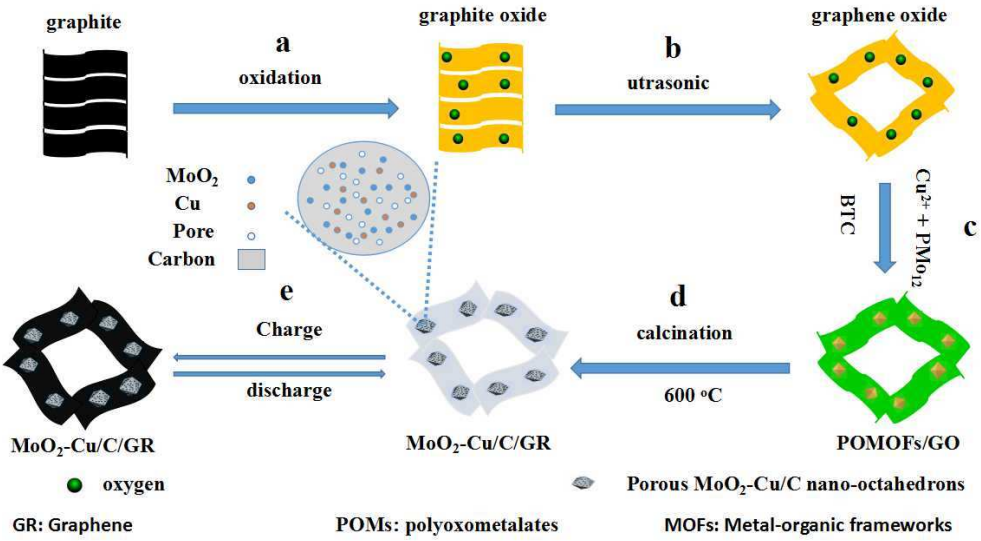

Scheme 1. Schematic of the synthesis procedure of porous MoO_2-Cu/C/GR nano-octahedrons.

Scheme 1 illustrates the synthesis process of GO and porous MoO_2-Cu/C/GR nano-octahedron quadruple nanocomposite via a facile one-pot chemical precipitation method followed with thermal treatment. The morphologies and diffraction peaks of the POMOF precursor were displayed in Fig. S1, which were well consistent with the crystal structure of POMOF previously reported [5, 50]. As shown in Scheme 1, the POMOF/GO was calcinated at 600 ^oC for 3 h under N_2 atmosphere. During the annealing process, the MoO_2 nanoparticles would form through the decomposition of Mo based POMs. Meanwhile, the Cu^{2+} clusters were reduced to Cu, a carbon network skeleton came into being from BTC ligands, and GO were reduced to GR. Finally, porous MoO_2-Cu/C/GR nano-octahedrons were obtained and then used as an anode material for lithium-ion batteries.

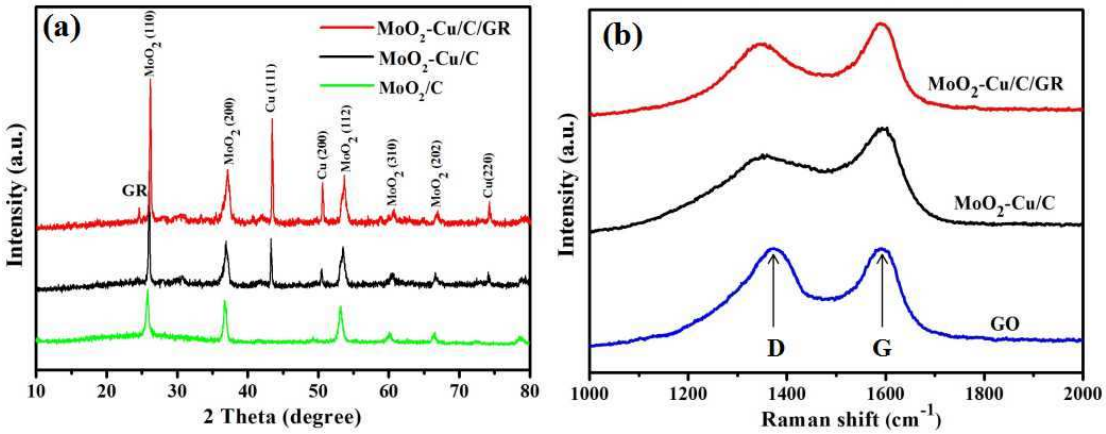

Fig. 1. (a) XRD patterns of MoO_2/C, MoO_2-Cu/C and MoO_2-Cu/C/GR. (b) Raman patterns of GO, MoO_2-Cu/C and MoO_2-Cu/C/GR.

Fig. 1a shows the XRD patterns of MoO_2/C, MoO_2-Cu/C and MoO_2-Cu/C/GR nano-octahedrons. Three strong peaks at 43.3^o, 50.4^o, and 74.1^o correspond to the (111), (200), and (220) crystal planes of Cu phase (JCPDS no. 85-1326), respectively. Diffraction peaks at 25.9^o, 37.2^o, 53.4^o, and 60.4^o are assigned to the (011), (200), (022) and (013) crystal planes of MoO_2 phase (JCPDS no.78-1071), respectively. A broad peak around 24.5^o appeared in the pattern of the as-prepared porous MoO_2-Cu/C/GR nano-octahedrons, being indexed to graphene. The Raman spectra of porous MoO_2-Cu/C/GR, porous MoO_2-Cu/C, GO samples are also shown in Fig. 1b.

The spectra display two prominent peaks at 1368 cm^{-1} (D bands) and 1592 cm^{-1} (G bands). It is well known that the intensity ratio of D to G bands (I_D/I_G) was used to probe the ordered and disordered crystal structures of carbon [51]. The smaller the I_D/I_G ratio, the higher the degree of ordering in the carbon material [52]. The I_D/I_G values of GO, MoO_2-Cu/C and MoO_2-Cu/C/GR composites are 0.88, 0.94, and 1.48, respectively. The I_D/I_G for MoO_2-Cu/C/GR is much larger than that for graphene oxide and MoO_2-Cu/C, showing the transformation of graphene sheets from graphene oxide after the calcination treatment. Hence, the Raman results correspond to the formation of MoO_2-Cu/C/GR composites.

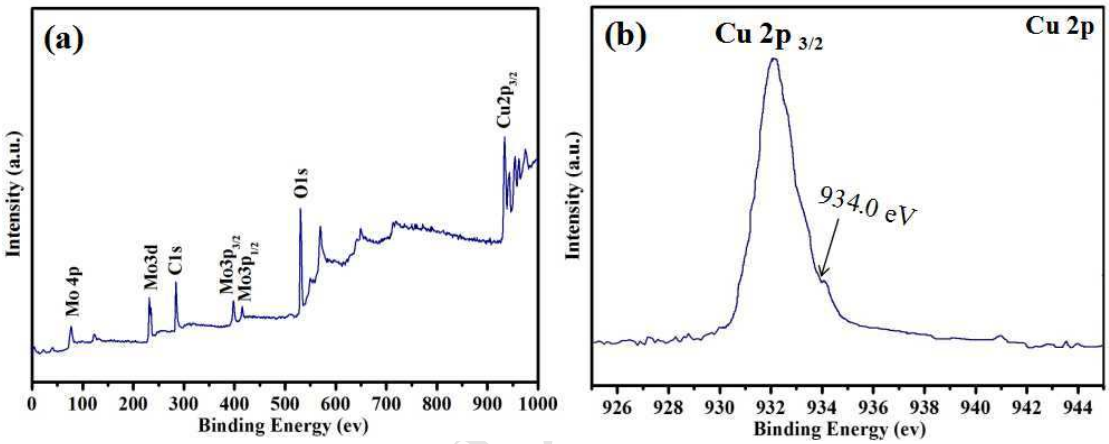

Fig. 2. (a) XPS survey scan of MoO_2-Cu/C/GR nano-octahedrons. (b) High-resolution XPS spectra of the Cu2p peak.

In order to explore the surface component of the products, XPS of porous MoO_2-Cu/C/GR nano-octahedrons was measured (Fig. 2a). A single $Cu2p_{3/2}$ peak appears at 932.5 eV (Fig. 2b) without a significant shoulder peak of 934.0 eV, indicating the nonexistence of Cu^{2+} [5, 53, 54]. It should be noted that Cu and Cu_2O could not be resolved by this deconvolution because their binding energies are very close [5]. The presence of Cu^0 can be confirmed by the above XRD patterns of MoO_2-Cu/C/GR and the lattice fringes of metallic Cu(111) planes of HRTEM. The high-resolution Mo3d spectrum (Fig. S2a) can be further deconvoluted into four individual peaks which located at 236.0, 232.9, 231.2, and 229.7 eV, corresponding to the Mo(VI)$3d_{3/2}$, Mo(IV)$3d_{3/2}$, Mo(VI)$3d_{5/2}$, and Mo(IV)$3d_{5/2}$, respectively [55]. Two

peaks centered at 232.9 and 229.7 eV are attributed to the oxidation states of MoO_2. Additionally, peaks at 236.0 and 231.2 eV are resulted from the slight surface oxidation of MoO_2 in air [56]. The high-resolution C1s XPS spectrum (Fig. S2b) depicts that three distinct C configurations coexist, including graphic carbon (C-C), carbon in C-O, and carbonyl carbon (C=O), respectively [57]. The presence of MoO_2 nanoparticles is further confirmed by the strong O1s peak at 530.2 eV corresponding to oxygen species in MoO_2 phase (Fig. S2c). Two small O1s peaks at 531.8 and 532.2 eV indicates the presence of residual oxygen-containing groups bonded with C atoms in graphene [58].

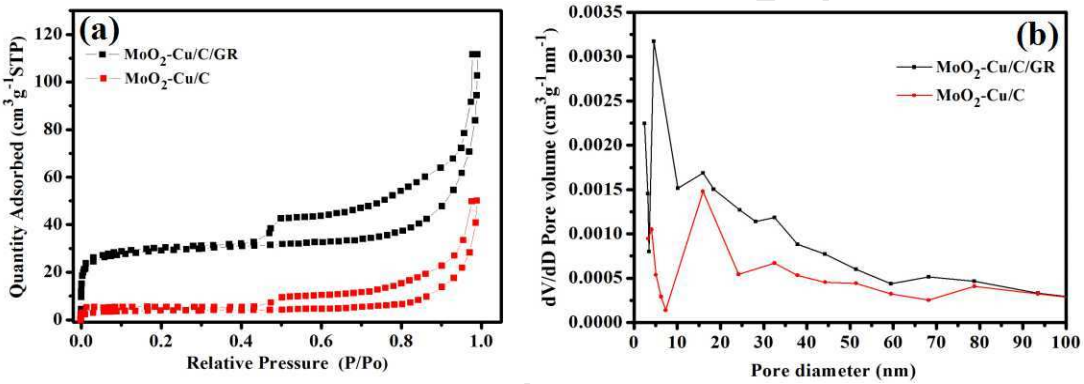

Fig. 3. (a) Nitrogen adsorption-desorption isotherms of MoO_2-Cu/C/GR and MoO_2-Cu/C. (b) Pore size distribution of MoO_2-Cu/C/GR and MoO_2-Cu/C.

The surface areas and pore structures of the porous MoO_2-Cu/C/GR product were further investigated by N_2 adsorption-desorption measurement. Fig. 3a exhibits the N_2 adsorption/desorption isotherms of the porous MoO_2-Cu/C/GR nano-octahedrons and porous MoO_2-Cu/C nano-octahedrons. They all exhibit typical type-IV features of absorbents with a H_2 hysteresis loop. The BET surface area is 107.17 m^2 g^{-1} for porous MoO_2-Cu/C/GR nano-octahedrons and 15.6 m^2 g^{-1} for porous MoO_2-Cu/C nano-octahedrons. Obviously, the BET specific surface area of MoO_2-Cu/C/GR is much higher than that of porous MoO_2-Cu/C, indicating that the introduction of graphene improve the BET area. For MoO_2-Cu/C nano-octahedrons, the primary pore size was mainly in the range of 7.3-24.1 nm, and the average pore

diameter is 15.94 nm (Fig. 3b). In contrast, the primary pore size of MoO_2-Cu/C/GR composite was in a narrow range of 3.4-10.1 nm, and the average pore diameter is 4.5 nm. This suggests that the graphene wrapped MoO_2-Cu/C nano-octahedrons formed uniform pores and channels for the nanocomposite. The obviously improved surface area endows porous MoO_2-Cu/C/GR nano-octahedrons with more lithium storage sites. It could be expected that the porous MoO_2-Cu/C/GR nano-octahedrons delivers a higher reversible capacity compared to MoO_2-Cu/C.

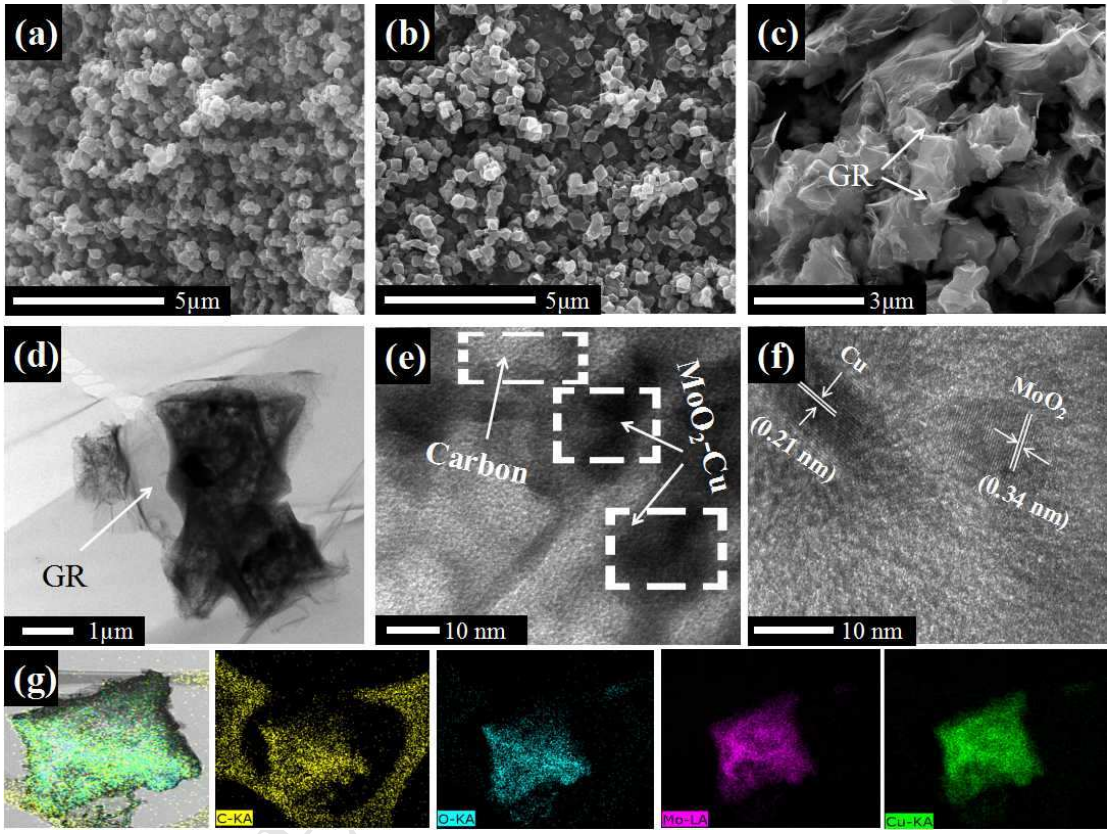

Fig. 4. (a) SEM image of MoO_2/C. (b) SEM image of MoO_2-Cu/C. (c) SEM image of MoO_2-Cu/C/GR. (d) TEM image of MoO_2-Cu/C/GR. (e, f) HRTEM images of MoO_2-Cu/C/GR. (g) Elemental mapping showing the uniform dispersion of C (yellow), O (blue), Mo (Pink) and Cu (green) elements in the nano-octahedrons.

The morphologies and sizes of MoO_2/C, MoO_2-Cu/C and MoO_2-Cu/C/GR nano-octahedrons were characterized by SEM. Fig. 4a and 4b exhibit the SEM images of the MoO_2/C and MoO_2-Cu/C nano-octahedrons. The as-synthesized product composed of graphene and MoO_2-Cu/C octahedrons (Fig. 4c). It is clearly seen that

the octahedrons are wrapped between graphene. To further investigate the microstructure, the porous MoO_2-Cu/C/GR product is characterized by TEM. TEM images of the porous MoO_2-Cu/C/GR nano-ctahedrons are exhibited in Fig. 4d. TEM characterization further confirms the intimate contact between the graphene and porous MoO_2-Cu/C octahedrons. HRTEM image of porous MoO_2-Cu/C/GR clearly reveal the presence of nano-octahedrons (Fig. 4e). It should be noted that the MoO_2-Cu nanoparticles labeled by a square are distributed in the carbon matrix. As shown in Fig. 4f, the presence of Cu nanocrystallites between MoO_2-Cu/C/GR grain is identified by the lattice fringes with an interspacing of 0.21 nm that is ascribed to the (111) planes of metallic Cu (d111 = 0.21 nm). And the lattice fringes with an interspacing distance of 0.34 nm is ascribed to MoO_2 [4]. The elemental mapping reveals the homogeneous distribution of C, O, Mo and Cu elements in the nano-octahedrons (Fig. 4g). The EDX results are consistent with those of XPS and further prove that the as-synthesized product is MoO_2-Cu/C/GR. In order to further clarify the carbon contents in the as-prepared materials, the TG and ICP measurements were also done. As seen in Fig. S3, the carbon content is estimated to be 11.4 %. According to the Mo content of ICP results, the MoO_2 content is about 78.8 wt% in the porous MoO_2-Cu/C/GR nano-octahedrons. Based on the above data, XRD, Raman, SEM, TEM, HRTEM, Elemental mapping, XPS, BET, TG and ICP, it can be concluded that the MoO_2-Cu/C/GR nano-octahedrons have been successfully synthesized.

3.2. Electrochemical performances of MoO_2-Cu/C/GR

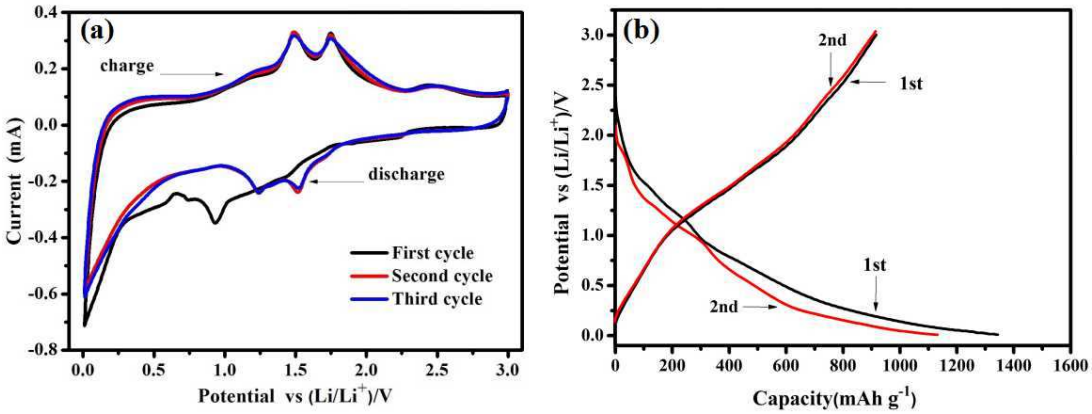

Fig. 5. (a) Cyclic voltammogram profiles for porous MoO_2-Cu/C/GR nano-octahedrons with the voltage range of 0.01-3 *vs* (Li/Li^+) V at 0.1 A g^{-1}.at 0.2 mV s^{-1} sweep rate. (b) The 1st and 2nd discharging-charging voltage profiles of porous MoO_2-Cu/C/GR nano-octahedrons anode at 0.1 A g^{-1}.

Fig. 5a exhibits the CV curves of MoO_2-Cu/C/GR anode for LIBs. In the first cathodic scan, the cathodic peak at 0.95 V can be ascribed to a phase transition from orthorhombic to monoclinic phase upon Li insertion as suggested by Dahn [59-60], as well as the formation of a solid electrolyte interface (SEI) film [61-63]. During the second and third cycle, two pairs of cathodic/anodic peaks at (1.23/1.48 V) and (1.52/1.73 V) represents two stages of reversible electrochemical lithium intercalation/deintercalation between monoclinic phase and reversible phase transition of partially lithiated Li_xMoO_2 [8, 9]. The Li^+ intercalation/deintercalation into/out of MoO_2 can be written as the following equ. 1 and 2 [8]. The peak current density was nearly unchanged in the 2nd and 3rd cycling, showing excellent capacity retentions.

$$xLi^+ + xe^- + MoO_2 \leftrightarrow Li_xMoO_2\ (0 \le x \le 0.98) \quad (1)$$

$$Li_{0.98}MoO_2 + 3.02Li \leftrightarrow 2Li_2O + Mo \quad (2)$$

Fig. 5b shows the representative charge/discharge curves of porous MoO_2-Cu/C/GR nano-octahedrons for the 1st and 2nd cycle with the voltage range of 0.01-3 *vs* (Li/Li^+) V at 0.1 A g^{-1}. In the first cycle, one short discharge plateau at approximately 0.95 V was observed, which was well consistent with the CV results. The capacity of porous MoO_2-Cu/C/GR nano-octahedrons depends on the total weight

including MoO_2 and carbon. The theoretical capacity of (*C*) the hypothetical mixture of MoO_2-Cu/C/GR is calculated as follows:

$C_{theoretical} = C_{MoO2} * \%_{mass\ of\ MoO2} + C_{carbon} * \%_{mass\ of\ carbon} + C_{Cu} * \%_{mass\ of\ Cu}$

$= 838 * 78.8\% + 372 * 11.2\% + 0 * 9.8\%$

$= 702\ mAh\ g^{-1}$

The porous MoO_2-Cu/C/GR nano-octahedrons deliver initial discharge/charge capacities of 1343.3 mAh g^{-1} and 937.8 mAh g^{-1} with coulombic efficiency of 69.8%, respectively. This gravimetric capacity is higher than the theoretical capacities of both MoO_2 (838 mAh g^{-1}) and carbon (372 mAh g^{-1}). This phenomenon is related to the larger electro-chemical active surface area of porous micro/nano-structures and the reversible growth of a polymer/gel-like layer on the surface of the MoO_2-Cu/C/GR active material or an interfacial lithium-storage [64-66]. On the other hand, the generated nanopores of MoO_2-Cu/C/GR could provide more active sites, which could increase the contact area between electrolyte and active materials, and improve the electron and ion transport. It should be noted that the first charge capacity is lower than that of discharge capacity. The capacity loss is ascribed to the irreversible reduction of MoO_2 to Mo, the formation of SEI film, and the decomposition of electrolyte, which are consistent with previous reports [6-9].

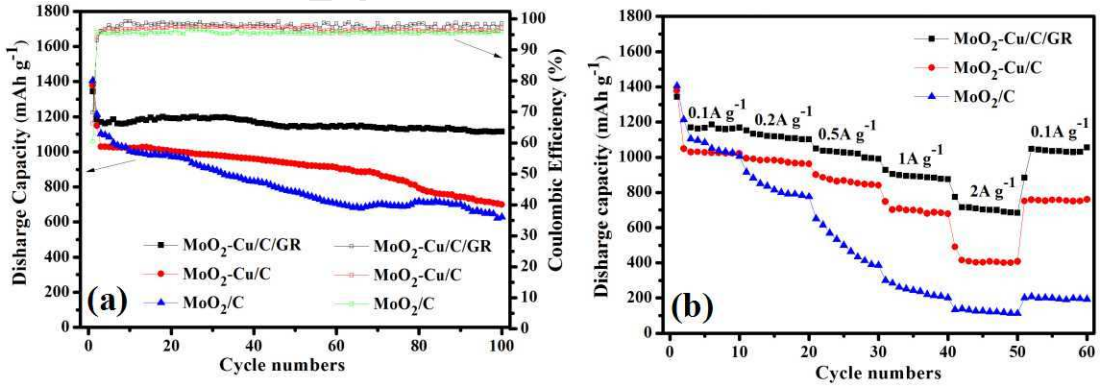

Fig. 6. (a) Cycling performances of MoO_2-Cu/C/GR, MoO_2-Cu/C, and MoO_2/C as anodes for LIBs at 0.1 A g^{-1}. (b) Rate capabilities of MoO_2-Cu/C/GR, MoO_2-Cu/C, and MoO_2/C at different rates.

Cycle performance is an important parameter for LIBs applications. Fig. 6a shows the comparisons of cycle performances of the MoO_2-Cu/C/GR, MoO_2-Cu/C and MoO_2/C samples at 0.1 A g^{-1}. It can be easily seen that with the increase of cycle numbers, the differences between MoO_2-Cu/C/GR, MoO_2-Cu/C and MoO_2/C sample became pronounced. At 100 cycles, the MoO_2-Cu/C delivered a 699.7 mAh g^{-1} discharge capacity with capacity retention of 53.8%, while the composite MoO_2-Cu/C/GR still keep a discharge capacity of 1114.8 mAh g^{-1} with capacity retention of 82.9% compared to the initial discharge capacity. The data of this work are also higher than other reported MoO_2 electrode materials (Table S1) [67-71]. On the other hand, the discharge capacity of MoO_2/C at 100^{th} cycle is about 629.1 mAh g^{-1}, which is lower than that of MoO_2-Cu/C composite (699.7 mAh g^{-1}). This result indicats that the copper phase helps to constrain the volumetric change and aggregation of active materials, and hence improve the electron transfer and the cyclic performance, which is similar to previous reports [35, 38]. To verify the stability of the electrode materials, the porous MoO_2-Cu/C/GR nano-octahedrons was characterized by SEM after 100 cycles at the current density of 0.1 A g^{-1} (Fig. 7). It can be clearly seen that the graphene and nano-octahedrons could retain original morphology and structure. These behaviors confirmed that the MoO_2-Cu/C/GR sample possesses a highly reversible structure stability during the lithium storage processes.

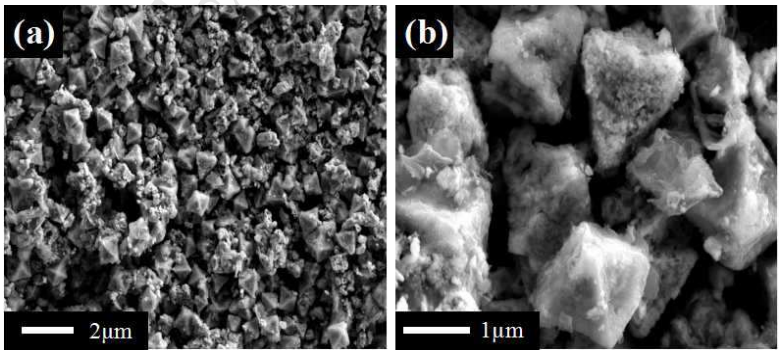

Fig. 7. (a, b) SEM images of porous MoO_2-Cu/C/GR nano-octahedrons after 100 cycles at the current density of 0.1 A g^{-1}.

In order to further investigate the roles of copper phase and graphene in the porous MoO_2-Cu/C/GR nano-octahedrons, the rate capabilities of the porous MoO_2-Cu/C/GR, MoO_2-Cu/C, and the MoO_2/C as anode materials for LIBs were also measured. As shown in Fig. 6b, the porous MoO_2-Cu/C/GR nano-octahedrons deliver the highest specific capacity among these samples. It is obvious that with the increase of the current rate, the differences of porous MoO_2-Cu/C/GR, MoO_2-Cu/C, and MoO_2/C became pronounced. The porous MoO_2-Cu/C/GR nano-octahedrons exhibit a discharge capacity of 1151 mAh g^{-1} at low rate of 0.1 A g^{-1}. When the charge-discharge rate increases to higher values of 1 A $g^{-1}$and 2 A g^{-1}, the discharge capacities maintained at 892.6 and 702.2 mAh g^{-1}, respectively, which are still much higher than that of MoO_2/C composite previously reported [4]. As comparison, the porous MoO_2-Cu/C sample exhibits lower discharge capacities of 680.5 mAh g^{-1} at 1 A g^{-1} rate and 400.4 mAh g^{-1} at 2 A g^{-1}. While the porous MoO_2/C product exhibits the lowest capacity. The superior rate behaviors of porous MoO_2-Cu/C/GR nano-octahedrons can be attributed to the following aspects. Firstly, the highly conductive Cu additives could not only significantly improve the surface intercalation reaction and reduce the cell polarization, but also enhance the electrical conductivity of electrode materials and thereby improve the rate capability. Secondly, graphene in the presence of porous MoO_2-Cu/C/GR nano-octahedrons not only accommodate the volume variations of MoO_2 nanoparticles, but also improve the electron transport property of the electrode material, resulting in lower charge transfer resistance and fast lithium ion diffusion compared to porous MoO_2-Cu/C nano-octahedrons [51].

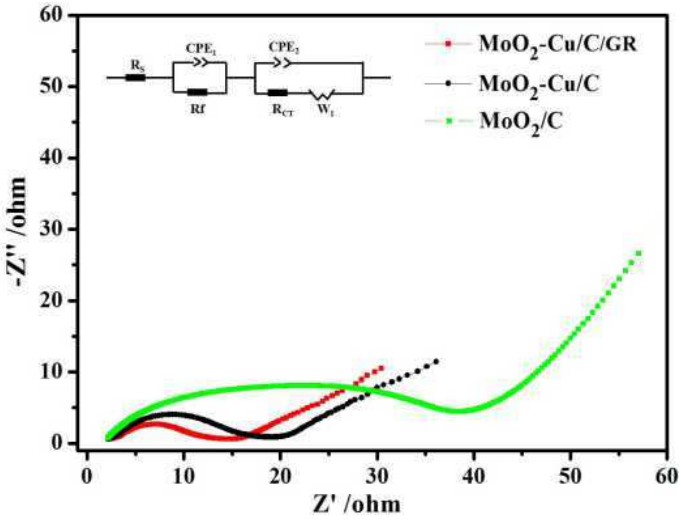

Fig. 8. EIS spectra of MoO_2-Cu/C/GR, MoO_2-Cu/C, and MoO_2/C applied as anode for LIBs after 10^{th} cycle. Inset shows the equivalent circuit.

For the purpose of further probing the rate capability, EIS were carried out using MoO_2-Cu/C/GR, MoO_2-Cu/C, and MoO_2/C as anodes for LIBs after 10^{th} cycle. Fig. 8 shows their EIS spectra which all composed of a depressed semicircle and a sloping line in the high-frequency and low-frequency region, respectively. The impedance plots were fitted by using the equivalent circuit model (Fig. 8 inset), which includes the electrolyte resistance Rs, the SEI resistance R_f, the charge-transfer resistance R_{ct}, the Warburg impedance (Zw) related to the diffusion of lithium ions into the bulk of the electrode materials, and two constant phase elements (CPE1 and CPE2) associated with the interfacial resistance and charge-transfer resistance, respectively. It can be seen that the charge transfer resistance of MoO_2-Cu/C is much smaller than that of MoO_2/C, showing that copper nanocrystallites could greatly reduce the charge-transfer impedance (*R*ct) of the electrode by forming a highly conductive network between metal oxide grains [35, 38]. In addition, the semicircle with the diameter of the porous MoO_2-Cu/C/GR composites is smaller than that of porous MoO_2-Cu/C. This result shows that the porous MoO_2-Cu/C/GR composites behave the lowest charge transfer resistance between the electrode and electrolyte interface（Rs). It is because that the GR as efficient charge carrier could facilitate charge transfer at the interface leading to higher rate capability, proving that the

porous MoO_2-Cu/C/GR nano-octahedrons possesses lower charge-transfer and contact impedance as anode for LIBs. These results are also in agreement with the superior rate capability of porous MoO_2-Cu/C/GR nano-octahedrons since charge transfer process is the rate determining step for conversion reactions [33].

4. Conclusions

In summary, porous MoO_2-Cu/C/GR nano-octahedrons have been successfully prepared via a facile one-pot chemical precipitation method followed with thermal treatment. As an advanced anode for LIBs, the porous MoO_2-Cu/C/GR nano-octahedrons deliver an excellent cycle performances (discharge capacity of 1114.8mAh g^{-1} at 0.1 A g^{-1} after 100 cycles with capacity retention of 82.9%) and enhanced rate capability (892.6 mAh g^{-1} and 702.2 mAh g^{-1} discharge capacity at 1 A g^{-1} and 2 A g^{-1} rate, respectively). The obvious enhancement can be attributed to the positive synergistic effect of MoO_2, carbon, copper phase and GR. This work highlights the advantages of the combination of MoO_2, copper phase, carbon, and GR for the maximum utilization of rate capability and capacity retentions. This work also supplies a simple way to prepare porous MoO_2-Cu/C/GR nano-octahedrons as an anode for high power LIBs.

Acknowledgment

This work was financially supported by the National Natural Science Foundation of China (21671185, 51672114), the Natural Science Foundation of the Jiangsu Higher Education Institution of China (14KJB150007), the Scientific Research Foundation for the Returned Overseas Chinese Scholars of State Education Ministry (2015311), the Marine Equipment and Technology Institute for Jiangsu University of Science and Technology (HZ20170015), and the State Key Laboratory of Structural Chemistry of Fujian Institute of Research on the Structure of Matter (20150020).

References

[1] Y. Sun, X. Hu, J. C. Yu, Q. Li, W. Luo, L. Yuan, W. Zhang, Y. Huang, Morphosynthesis of a hierarchical MoO_2 nanoarchitecture as a binder-free anode for

lithium-ion batteries, *Energy Environ. Sci*. 4(2011)2870-2877.

[2] X. Zhang, X. Song, S. Gao, Y. Xu, X. Cheng, H. Zhao, L. Huo, Facile synthesis of yolk-shell MoO_2 microspheres with excellent electrochemical performance as a Li-ion battery anode, *J. Mater. Chem. A* 1(2013)6858-6864.

[3] Y. Sun, X. Hu, W. Luo, Y. Huang, Self-assembled hierarchical MoO_2/graphene nanoarchitectures and their application as a high-performance anode material for lithium-ion batteries, *ACS Nano* 5(2011)7100-7107.

[4] G. Xia, D. Liu, F. Zheng, Y. Yang, J. Su, Q. Chen, Preparation of porous MoO_2@C nano-octahedrons from a polyoxometalate-based metal-organic framework for highly reversible lithium storage, *J. Mater. Chem. A* 4(2016)12434-12441.

[5] Y.D. Zhang, B.P. Lin, Y. Sun, P. Han, J.C. Wang, X.J. Ding, X.Q. Zhang, H. Yang, MoO_2@Cu@C composites prepared by using polyoxometalates@metal-organic frameworks as template for all-solid-state flexible supercapacitor, *Electrochim. Acta* 188(2016)490-498.

[6] Y. Sun, X. Hu, W. Luo, Y. Huang, Self-assembled hierarchical MoO_2/graphene nanoarchitectures and their application as a high-performance anode material for lithium-ion batteries, *ACS Nano* 5(2011)7100-7107.

[7] L. Yang, L. Liu, Y. Zhu, X. Wang,Y. Wu, Preparation of carbon coated MoO_2 nanobelts and their high performance as anode materials for lithium ion batteries, *J. Mater. Chem.* 22(2012)13148-13152.

[8] X. Zhang, X. Song, S. Gao, Y. Xu, X. Cheng, H. Zhao, L. Huo, Facile synthesis of yolk-shell MoO_2 microspheres with excellent electrochemical performance as a Li-ion battery anode, *J. Mater. Chem. A*1(2013)6858-6864.

[9] S. Hu, F. Yin, E. Uchaker, W. Chen, M. Zhang, J. Zhou, Y. Qi , G. Cao, Facile and green preparation for the formation of MoO_2-GO composites as anode material for lithium-ion batteries, *J. Phys. Chem. C* 118(2014)24890-24897.

[10] J.S. Cho, Y.J. Hong, Y.C. Kang, Design and synthesis of bubble-nanorod-structured Fe_2O_3-carbon nanofibers as advanced anode material for Li-ion batteries, *ACS Nano*, 9 (2015)4026-4035.

[11] M.C. Sun, M.F. Sun, H.X. Yang, W.H. Song, Y. Nie, S.N. Sun, Porous Fe_2O_3

nanotubes as advanced anode for high performance lithium ion batteries, *Ceram. Int*. 43(2017)363-367.

[12] X. Lou, J. Huang, T. Li, Hydrothermal synthesis of Fe_3O_4 and α-Fe_2O_3 nanocrystals as anode electrode materials for rechargeable Li-ion batteries, *J. Mater. Sci. Mater. Electron.* 25(2014)1193-1196.

[13] Y.Y. Chen, R. Cai, Y. Yang, C. Liu, A.H. Yuan, H.X. Yang, X.P. Shen, Cyanometallic frameworks derived hierarchical porous Fe_2O_3/NiO microflowers with excellent lithium-storage property, *J. Alloys Compd.* 698(2017)469-475.

[14] L.M. Zhang, B. Yan, J.H. Zhang, Y.J. Liu, A.H. Yuan, G. Yang, Co_3O_4 nanomaterials in lithium-ion batteries and gas sensors, *Ceram. Int.* 42(2016)5160-5170.

[15] Y. Wang, F. Yan, S.W. Liu, A.Y.S. Tan, H. Song, X.W. Sun, H.Y. Yang, Onion-like carbon matrix supported Co_3O_4 nanocomposites: a highly reversible anode material for lithium ion batteries with excellent cycling stability, *J. Mater. Chem. A.*1(2013)5212-5216.

[16] Y.Y. Chen, Y. Wang, H.X. Yang, H. Gan, X.W. Cai, X.M. Guo, B. Xu, M.F. Lü, A.H. Yuan, Facile synthesis of porous hollow Co_3O_4 microfibers derived-from metal-organic frameworks as an advanced anode for lithium ion batteries, *Ceram. Int.* 43(2017)9945-9950.

[17] H.X. Yang, Y. Wang, Y. Nie, S.N. Sun, T.Y. Yang, Co_3O_4/porous carbon nanofibers composite as anode for high performance lithium ion batteries with improved cycle performance and lithium storage capacity, *J. Compos. Mater.* 51(2017)215-222.

[18] X.M. Yin, C.C. Li, M. Zhang, Q.Y. Hao, S. Liu, L.B. Chen , T.H. Wang, One-step synthesis of hierarchical SnO_2 hollow nanostructures via self-assembly for high power lithium ion batteries, *J. Phy. Chem. C.* 114(2010)8084-8088.

[19] M.S. Park, G.X. Wang, Y.M. Kang, D. Wexler, S.X. Dou, H.K. Liu, Preparation and Electrochemical Properties of SnO_2 Nanowires for Application in Lithium−Ion Batteries, *Angew. Chem.* 46(2007)750-753.

[20] H.X. Yang, T. Song, S. Lee, H. Han, F. Xia, A. Devadoss, W. Sigmund, U. Paik,

Tin indium oxide/graphene nanosheet nanocomposite as an anode material for lithium ion batteries with enhanced lithium storage capacity and rate capability, *Electrochim. Acta* 91(2013)275-281.

[21] X.H. Huang, X.H. Xia, Y.F. Yuan, F. Zhou, Porous ZnO nanosheets grown on copper substrates as anodes for lithium ion batteries, *Electrochim. Acta* 56(2011)4960-4965.

[22] H. Wang, Q. Pan, Y. Cheng, J. Zhao , G. Yin, Evaluation of ZnO nanorod arrays with dandelion-like morphology as negative electrodes for lithium-ion batteries, *Electrochim. Acta.* 54(2009)2851-2855.

[23] S. Gao, S. Yang, J. Shu, S. Zhang, Z. Li, K. Jiang, Green fabrication of hierarchical CuO hollow micro/nanostructures and enhanced performance as electrode materials for lithium-ion batteries, *J. Phys.Chem. C* 112(49)(2008)19324-19328.

[24] J.Y. Xiang, J.P. Tu, L. Zhang, Y. Zhou, X.L. Wang, S.J. Shi, Self-assembled synthesis of hierarchical nanostructured CuO with various morphologies and their application as anodes for lithium ion batteries, *J. Power Sources* 195(2010)313-319.

[25] H. Liu, Z. Bi, X.G. Sun, R.R. Unocic, M.P. Paranthaman, S. Dai, G.M. Brown, Mesoporous TiO_2-B microspheres with superior rate performance for lithium ion batteries, *Adv. Mater.* 23(2011)3450-3454.

[26]S. Liu, H. Jia, L. Han, J. Wang, P. Gao, D. Xu, S. Che, S. Che, Nanosheet-constructed porous TiO_2-B for advanced lithium ion batteries, *Adv. Mater.* 24(2012)3201-3204.

[27] X. Lang, A. Hirata, T. Fujita, M. Chen, Nanoporous metal/oxide hybrid electrodes for electrochemical supercapacitors, *Nat. Nanotechnol.* 6(2011)232-236.

[28] L.W. Liang, C. Wu, X.F. Sun, X. Sun, L.R. Hou, J.F. Sun, C.Z. Yuan, Sur-/interface engineering of hierarchical $LiNi_{0.6}Mn_{0.2}Co_{0.2}O_2$@$LiCoPO_4$@graphene architectures as promising high-voltage cathodes toward advanced Li-ion batteries, *Adv. Mater. Inter.* 2017, 1700382, DOI: 10.1002/admi.201700382.

[29] H.X. Yang, Y. Xie, Y. Wang, B. Wu, Y.Y. Chen, B. Xu, Green synthesis of $[(C_4H_9)_4N]_3[PMo_{12}O_{40}]$/Graphene Nanosheets Nanocomposites as advanced cathode for high performance lithium ion batteries, *Nano-Structures & Nano-Objects* 11

(2017)76-81.

[30] H.X. Yang, X. Liu, S. Sun, Y. Nie, H.P. Wu, T.Y. Yang, S. Zheng, S. Lin, Green and facile synthesis of graphene nanosheets/$K_3PW_{12}O_{40}$ nanocomposites with enhanced photocatalytic activities, *Mater. Res. Bull.* 78(2016)112-118.

[31] X.Y. Liu, Y. Nie, H.X. Yang, S.N. Sun, Y.Y. Chen, T.Y. Yang, S.L. Lin, Enhancement of the photocatalytic activity and electrochemical property of graphene-$SrWO_4$ nanocomposite, *Solid State Sci.* 55(2016)130-137.

[32] W. Bei, W. Ying, J. Park, H. Ahn, G. Wang, In situ synthesis of Co_3O_4/graphene nanocomposite material for lithium-ion batteries and supercapacitors with high capacity and supercapacitance, *J. Alloys Compd.* 509(2011)7778-7783.

[33] H.X. Yang, L. Li, Tin-indium/graphene with enhanced initial coulombic efficiency and rate performance for lithium ion batteries, *J. Alloys Compd.* 584(2014) 76-80.

[34] S. Liang, X. Zhu, P. Lian, W. Yang, H. Wang, Superior cycle performance of Sn@C/graphene nanocomposite as an anode material for lithium-ion batteries, *J. Solid State Chem.* 184(2011)1400-1404.

[35] S. Huang, Z. Wen, B. Lin, J. Han ,X. Xu,The high-rate performance of the newly designed $Li_4Ti_5O_{12}$/Cu composite anode for lithium ion batteries, *J. Alloys Compd.* 457(2008)400-403.

[36] Q. Xie, Y. Ma, D. Zeng, X. Zhang, L. Wang, G. Yue, D. L. Peng, Hierarchical ZnO-Ag-C composite porous microspheres with superior electrochemical properties as anode materials for lithium ion batteries, *ACS App. Mater. Inter.* 6(2014)19895-19904.

[37] G.X. Pan, X.H. Xia, F. Cao, J. Chen ,Y.J. Zhang, Construction of Co/Co_3O_4-C ternary core-branch arrays as enhanced anode materials for lithium ion batteries, *J. Power Sources* 293(2015)585-591.

[38] J.S. Zhu, G.Z. Hu, J. Zhang, Preparation of Sn-Cu-graphene nanocomposites with superior reversible lithium ion storage, *Mater. Lett.* 185(2016)565-568.

[39] H.B. Wu, B.Y. Xia, L. Yu, X. Y. Yu, X.W. Lou, Porous molybdenum carbide nano-octahedrons synthesized via confined carburization in metal-organic frameworks

for efficient hydrogen production, *Nat. Commun.* 6(2015)6512-9518.

[40] L. Zhang, B.Q. Shan, H.X. Yang, D.S. Wu, R. Zhu, J.H. Nie, R. Cao, A new heterogeneous photocatalyst based on Wells-Dawson polyoxometalate and nickel coordination compounds: synthesis, structure and property, *RSC Adv.* 5(2015)23556-23562.

[41] H.X. Yang, J.C. Meng, X.F. Sun, L.Z. Chen, D. Yang, A new three-dimensional organic-inorganic hybrid constructed from Keggin polyoxometalates and Cu^{I}-pyrazine coordination polymers , *Inorg. Chem. Commun.* 39(2014)43-46.

[42] H.X. Yang, B.Q. Shan, L. Zhang, A new composite membrane based on Keggin polyoxotungstate/poly(vinylidene fluoride) and its application in photocatalysis, *RSC Adv.* 4(2014)61226-61231.

[43] T. Wei, M. Zhang, P. Wu, Y.J. Tang, S.L. Li, F.C. Shen, X.L. Wang, X.P. Zhou, Y.Q. Lan, POM-based metal-organic framework/reduced graphene oxide nanocomposites with hybrid behavior of battery-supercapacitor for superior lithium storage, *Nano Energy* 34 (2017)205-214.

[44] Y.Y. Wang, M. Zhang, S.L. Li, S.R. Zhang, W. Xie, J.S. Qin, Z.M. Su, Y.Q. Lan, Diamondoid-structured polymolybdate-based metal-organic frameworks as high-capacity anodes for lithium-ion batteries, *Chem. Commun.* 53(2017)5204-5207.

[45] X.Y. Yang, T. Wei, J.S. Li, N. Sheng, P.P. Zhu, J.Q. Sha, T. Wang, and Y.Q. Lan, Polyoxometalate-incorporated metallapillararene/metallacalixarene metal-Organic frameworks as anode materials for lithium ion batteries, Inorg. Chem. 56(2017)8311-8318.

[46] Q. Huang, T. Wei, M. Zhang, L.Z. Dong, A.M. Zhang, S.L. Li, W.J. Liu, J. Liu and Y.Q. Lan, A highly stable polyoxometalate-based metal-organic framework with p-p stacking for enhancing lithium ion battery performance, J. Mater. Chem. A 5(2017)8477-8483.

[47] Y.D. Zhang, B.P. Lin, , J.C. Wang, P. Han, T. Xu, Y. Sun, X.Q. Zhang, H. Yang, Polyoxometalates@metal-Organic frameworks derived porous MoO_3@CuO as electrodes for symmetric all-solid-state supercapacitor, Electrochim. Acta 191(2016)795-804.

[48] J.S. Li, Y. Wang, C.H. Liu, S.L. Li, Y.G. Wang, L.Z. Dong, Z.H. Dai, Y.F. Li, Y.Q. Lan, Coupled molybdenum carbide and reduced graphene oxide electrocatalysts for efficient hydrogen evolution, *Nat. Commun.* 7(2016)11204.

[49] H. Gong, Y. Zhu, L.Wang, D.Wei, J. Liang, Y. Qian, Solid-state synthesis of uniform Li_2MnSiO_4/C/graphene composites and their performance in lithium-ion batteries, *J. Power Sources* 246(2014)192-197.

[50] C.Y. Sun , S.X. Liu , D.D. Liang , K.Z. Shao, Y.H. Ren, Z.M. Su, Highly stable crystalline catalysts based on a microporous metal-organic framework and polyoxometalates, *J. Am. Chem. Soc*. 131(2009)1883-1888.

[51] H. Li , C. Lu, B. Zhang, A straightforward approach towards Si@C/graphene nanocomposite and its superior lithium storage performance, *Electrochim. Acta 120*(2014)96-101.

[52] Y. Shi , S.L. Chou, J.Z. Wang, D. Wexler, H. J. Li, H. K. Liu, Y. Wu. Graphene wrapped $LiFePO_4$/C composites as cathode materials for Li-ion batteries with enhanced rate capability, *J. Mater. Chem. 22* (2012)16465-16470.

[53] F. Alonso , T. Melkonian , Y. Moglie, M. Yus, Homocoupling of terminal alkynes catalysed by ultrafine copper nanoparticles on titania, *Eur. J. Org. Chem*. 13 (2011)2524-2530.

[54] I. Platzman , R. Brener , H. Haick and R. Tannenbaum, Oxidation of polycrystalline copper thin films at ambient conditions, *J. Phy. Chem. C*. 112 (2008)1101-1108.

[55] Y. Zhou, Q. Liu, D. Liu, H. Xie, G. Wu, W. Huang, Carbon-coated MoO_2, dispersed in three-dimensional graphene aerogel for lithium-ion battery, *Electrochim. Acta* 174(2015)8-14.

[56] K. Palanisamy, Y. Kim, H. Kim, M. K. Ji, W. S. Yoon, Self-assembled porous MoO_2/graphene microspheres towards high performance anodes for lithium ion batteries, *J. Power Sources* 275(2015)351-361.

[57] Y. Yamada , H. Yasuda, K. Murota, M. Nakamura, T. Sodesawa, S. Sato, Analysis of heat-treated graphite oxide by x-ray photoelectron spectroscopy, *J. Mater. Sci*. 48(2013)8171-8198.

[58] S. Qiu, G. Lu, J. Liu, H. Lyu, C. Hu, B. Li, X. Yan, J. Guo, Enhanced electrochemical performances of MoO_2 nanoparticles composited with carbon nanotubes for lithium-ion battery anodes *RSC Adv.* 5(2015)87286-87294.

[59] J.R. Dahn and W.R. McKinnon, Structure and electrochemistry of $LixMoO_2$ *Solid State Ionics 23*(1987)1-7.

[60] L. Zhou , H. B. Wu , Z. Wang, X.W. Lou, Interconnected MoO_2 nanocrystals with carbon nanocoating as high-capacity anode materials for lithium-ion batteries *ACS App. Mater. Interfaces.* 3(2011)4853-4857.

[61] Y.Y. Chen, Y. Wang, H.X. Yang, H. Gan, X.W. Cai, X.M. Guo, B. Xu, M.F. Lü, A.H. Yuan, Facile synthesis of porous hollow Co_3O_4 microfibers derived-from metal-organic frameworks as an advanced anode for lithium ion batteries, *Ceram. Int.* 43 (2017)9945-9950.

[62] H.X. Yang, T. Song, L. Liu, A. Devadoss, F. Xia, H. Han, H. Park, W. Sigmund, K. Kwon, U.Y. Paik, Polyaniline/polyoxometalate hybrid nanofibers as cathode for lithium ion batteries with improved lithium storage capacity, *J. Phy. Chem. C.* 117(2013)17376-17381.

[63] S.N. Sun, Y. Nie, M. Sun, T. Liang, M.C. Sun, H.X. Yang, Facile synthesis of $CoNi_2S_4$ one-dimensional nanorods as anode for high performance lithium ion batteries, *Mater. Lett.* 176(2016)87-9.

[64] S. Laruelle, S. Grugeon, P. Poizot, M. Dolle, L. Dupont, J.M. Tarascon On the origin of the extra electrochemical capacity displayed by MO/Li cells at low potential, *J. Electrochem. Soc.* 149(2002)A627-A634.

[65] Y.Z. Jiang, D. Zhang, Y. Li, T.Z. Yuan, N. Bahlawane, C. Liang, W.P. Sun, Y.H. Lu, M. Yan, Amorphous Fe_2O_3 as a high-capacity, high-rate and long-life anode material for lithium ion batteries, *Nano Energy* 4(2014)23-30.

[66] X.J. Jiang, W. Yu, H. Wang, H.Y. Xu, X.Z. Liu, Y. Ding, Enhancing the performance of MnO by double carbon modification for advanced lithium-ion battery anodes, *J. Mater. Chem. A* 4(2016)920-925.

[67] S. Wang, B. Liu, G. Zhi, G. Xu, Q. Wang, J. Zhang, 2D layered mesoporous MoO_2/rGO composites for high performance anode materials in lithium-ion

battery, *Microporous Mesoporous Mater*. 246(2017)14-23.

[68] C. Zhang, P. Zhang, J. Dai, H. Zhang, A. Xie, Y. Shen, Facile synthesis and electrochemical properties of MoO_2/reduced graphene oxide hybrid for efficient anode of lithium-ion battery, *Ceram. Int*. 42(2016)3618-3624.

[69] X. Liu, W. Ji, J. Liang, L. Peng, W. Hou, MoO_2@carbon hollow microspheres with tunable interiors and improved lithium-ion battery anode properties, Phys. *Chem. Chem. Phys.* 16(2014)20570-20577.

[70] Q. Tang, Z. Shan, L. Wang and X. Qin, MoO_2-graphene nanocomposite as anode material for lithium-ion batteries, *Electrochim. Acta*. 79(2012)148-153.

[71] F. Xia, X. Hu, Y. Sun, W. Luo, Y. Huang, Layer-by-layer assembled MoO_2-graphene thin film as a high-capacity and binder-free anode for lithium-ion batteries, *Nanoscale* 4(2012)4707-4711.

Figure captions:

Fig. 1. (a) XRD patterns of MoO_2/C，MoO_2-Cu/C and MoO_2-Cu/C/GR. (b) Raman patterns of GO, MoO_2-Cu/C and MoO_2-Cu/C/GR.

Fig. 2. (a) XPS survey scan of MoO_2-Cu/C/GR nano-octahedrons. (b) High-resolution XPS spectra of the Cu2p peak.

Fig. 3. (a) Nitrogen adsorption-desorption isotherms of MoO_2-Cu/C/GR and MoO_2-Cu/C. (b) Pore size distribution of MoO_2-Cu/C/GR and MoO_2-Cu/C.

Fig. 4. (a) SEM image of MoO_2/C. (b) SEM image of MoO_2-Cu/C. (c) SEM image of MoO_2-Cu/C/GR. (d) TEM image of MoO_2-Cu/C/GR. (e, f) HRTEM images of

MoO_2-Cu/C/GR. (g) Elemental mapping showing the uniform dispersion of C (yellow), O (blue), Mo (Pink) and Cu (green) elements in the nano-octahedrons.

Fig. 5. (a) Cyclic voltammogram profiles for porous MoO_2-Cu/C/GR nano-octahedrons at 0.2 mV s^{-1} sweep rate. (b) The 1st and 2nd discharging-charging voltage profiles of porous MoO_2-Cu/C/GR nano-octahedrons anode at 0.1 A g^{-1}.

Fig. 6. (a) Cycling performances of MoO_2-Cu/C/GR, MoO_2-Cu/C, and MoO_2/C as anodes for LIBs at 0.1 A g^{-1}. (b) Rate capabilities of MoO_2-Cu/C/GR, MoO_2-Cu/C, and MoO_2/C at different rates.

Fig. 7. (a, b) SEM images of porous MoO_2-Cu/C/GR nano-octahedrons after 100 cycles at the current density of 0.1 A g^{-1}.

Fig. 8. EIS spectra of MoO_2-Cu/C/GR, MoO_2-Cu/C, and MoO_2/C applied as anode for LIBs after 10th cycle. Inset shows the equivalent circuit.

Scheme caption

Scheme 1. Schematic of the synthesis procedure of porous MoO_2-Cu/C/GR nano-octahedrons.

Highlights:

► A new porous MoO_2-Cu/C/graphene nanocomposite was firstly synthesized.

► MoO_2-Cu/C/graphene nanocomposite delivers excellent rate capability.

► Copper phase and graphene play an important role in rate capability.